Simulating a High-speed Abrasive Particle Impacting on a Tensile Block Using SPH-FEM

Yanjie Liu
Shanghai Key Lab of Intelligent Manufacturing and Robotic, School of Mechatronic Engineering and Automation, Shanghai University, Shanghai, China

Yue Zhao
School of Software, Northwestern Polytechnical University, Xian, China,

Kenji Yoshigoe
Faculty of Information Networking for Innovation and Design, Toyo University, Tokyo, Japan

Shijin Zhang (zhangshij@hotmail.com)
School of Software, Northwestern Polytechnical University, Xian, China,

Ming Chen
Shanghai Key Lab of Intelligent Manufacturing and Robotic, School of Mechatronic Engineering and Automation, Shanghai University, Shanghai, China

Research Article

Keywords: SPH-FEM, Abrasive waterjet, Erosion damage, Johnson-Cook

Posted Date: March 23rd, 2021

DOI: https://doi.org/10.21203/rs.3.rs-332088/v1

Version of Record: A version of this preprint was published at The International Journal of Advanced Manufacturing Technology on July 12th, 2021. See the published version at https://doi.org/10.1007/s00170-021-07575-5.

Simulating a high-speed abrasive particle impacting on a tensile block using SPH-FEM

Yanjie Liu[1] Yue Zhao[2] Kenji Yoshigoe[3] Shijin Zhang[2] Ming Chen[1]

✉ Shijin Zhang

zhangshij@hotmail.com

[1] Shanghai Key Lab of Intelligent Manufacturing and Robotic, School of Mechatronic Engineering and Automation, Shanghai University, Shanghai, China, 200072

[2] School of Software, Northwestern Polytechnical University, Xian, China, 710129

[3] Faculty of Information Networking for Innovation and Design, Toyo University, Tokyo, Japan, 115-0053

Abstract

In recent years, more and more researches have been carried out on the erosion mechanism of abrasive particles on target materials in the abrasive waterjet cutting process. However, the effect of material property factors on the target erosion damage is rarely studied systematically. In this work, a 3D smoothed particle hydrodynamics-finite elements model is established for the simulation. The controlled variable method is used to study how each material property factor affects the erosion process of single abrasive particle and to find out the key material property factors of Al6061-T6 and Ti-6Al-4V. The influence of the interaction of the key material property factors on the target erosion damage is further evaluated using the orthogonal test method.

Keywords SPH-FEM · Abrasive waterjet · Erosion damage · Johnson-Cook

Declarations:

Funding

This paper is sponsored by the National Natural Science Foundation of China (52075313).

Competing interests (Not applicable)

Availability of data and materials

The datasets generated during and/or analyzed during the current study are available from the corresponding author on reasonable request.

Authors contributions (Not applicable)

Additional declarations for articles in life science journals that report the results of studies involving humans and/or animals.

Ethical approval (Not applicable)

Consent to participate (Not applicable)

Consent for publish (Not applicable)

1 Introduction

Erosion wear caused by solid particles is a phenomenon commonly happening in the industries of mechanical processing, mining, and constructing. Based on the idea that utilizes solid particles erosion instead of eliminating it, one of the promising and innovative machining technologies called

abrasive waterjet (AWJ) cutting is proposed by Hashish in early 1980s [1]. As the only cold high-energy beam processing technology in the world today, AWJ cutting has numerous benefits like no thermal distortion, high level of mobility, narrow kerf width, negligible heat effected zone, small cutting forces, etc. [2-4]. Almost all engineering materials can be cut by AWJ, especially the advanced difficult-to-cut materials such as ceramics [5]. Due to the specific characteristics of AWJ cutting, this processing technology has been used extensively in various industries in the past two decades.

In the AWJ cutting process, the erosion process is induced by the impact of the abrasive particles accelerated by high-speed water, which is regarded as a carrier. When the plastic deformation caused by the cumulative erosion of the abrasive particles on ductile target material reaches the tensile limit of the material, the removal of the workpiece material by the abrasive particles is realized.

A lot of work has been done to reveal the mechanism of hard particles eroding the target. Based on the theoretical analysis and experiments, two empirical erosion analytical mathematical models for ductile materials are developed by Finnie [6] and Bitter [7-8]. It is found that the erosion rate is related to the impact angle, impact velocity and material property factors such as the flow stress, the density of the target, etc. However, these models only coincide with the low-impact angle experiments of ductile materials [9]. Hutchings finds that the critical strain and dynamic hardness are also the main erosion parameters that influence the erosion rate [10]. Several experiments are conducted by Sundararajan, who also finds that particle shape and specific heat capacity of the target have an effect on erosion of ductile materials [11-12]. Li WY et al. use finite element method to simulate the impacts of ultrahigh velocity micro-particles on steels and find that the material removal process is associated with the magnitude of the plastic strain, the flow stress and thermal conditions [13]. Mieszala M et al. report that the erosion rate of the target material is positively correlated with the grain size and negatively correlated with the hardness. And it is related to the Young's modulus of the target material [14]. Barabas SA et al. notice that the machinability is influenced by other factors like the hardness and the microstructure of the removed material [15]. However, although the relationship between the erosion mechanism of ductile materials and certain material property factors has been studied by a lot of theoretical analysis and experiments, it is still not clear.

In the AWJ cutting process, the cutting quality and accuracy are directly affected by the material property factor of the workpiece material. However, the existing cutting model evades the crucial point and the combined effect of all material property factors is replaced by a single parameter named as machinability [16]. Therefore, in the current study, by studying how each material property factor affects the erosion process of single abrasive particle, the key material property factors could be found out for the ductile materials (Al6061-T6 and Ti-6Al-4V) by establishing a 3D smoothed particle hydrodynamics-finite elements model (SPH-FEM) [17-18] in ANSYS/LS-DYNA software. The study of the mechanisms of single abrasive eroding the target is of critical importance in the advancement of the AWJ cutting technique.

2 Smoothed particle hydrodynamics-finite elements model

The distortion and tangling of Lagrange mesh of the impacted area, which can cause calculation errors, are caused by the great kinetic energy of a high-speed abrasive particle during large

deformation. A large amount of time is spent on the calculation process using SPH method, and smooth particles are not easily added with boundary conditions. As a result, SPH-FEM mothed is proposed to take advantages of each mothed in this paper. The coupling method is used to study the dynamic behavior when abrasive particles impact the target, which contributes to a better understanding erosion mechanism of the target materials.

2.1 Material model and equation of state

The Johnson-Cook (J-C) constitutive model [19] with Gruneisen equation of state (EOS) [20] is employed to describe the response of the target materials to large deformation and high strain rate. In the J-C model, the functional relationship among the von Mises flow stress σ_f for ductile materials, yield stress constant A, strain hardening constant B, effective plastic strain $\bar{\varepsilon}^P$, strain rate $\dot{\varepsilon}^*$, and homologous temperature T^* is given by

$$\sigma_f = \left(A + B\bar{\varepsilon}^{P\,n}\right)(1 + c\ln\dot{\varepsilon}^*)(1 - T^{*m}) \tag{1}$$

where n, c, and m are input constants; $T^* = (T - T_{room})/(T_{melt} - T_{room})$; T, T_{room}, and T_{melt} are the workpiece temperature, the room temperature, and the melting point of the workpiece, respectively.

In our work, the J-C shear failure model is adopted to study the damage behavior of the target materials. The failure criterion is described as the fracture occurs when the value of the damage parameter $D = \sum \Delta\bar{\varepsilon}^P/\varepsilon^f$ reaches 1. The strain ε^f at fracture is defined as

$$\varepsilon^f = (D_1 + D_2 exp D_3\sigma^*\ )(1 + D_4\ln\dot{\varepsilon}^*)(1 + D_5 T^*) \tag{2}$$

where D_1~D_5 are failure parameters and σ^* is the ratio of pressure divided by effective stress.

Table 1 Material constants of Al6061-T6 and Ti-6Al-4V [21-23]

Materials properties	Symbol	Al6061-T6	Ti-6Al-4V
Density	ρ	$2800\ kg/m^3$	$4428\ kg/m^3$
Shear modulus	G	$26\ GP_a$	$41.9\ GP_a$
Poisson's ratio	ν	0.33	0.31
Melting temperature	T_{melt}	$925\ K$	$1878\ K$
Specific heat	C_P	$875\ J/(kg\cdot K)$	$580\ J/(kg\cdot K)$
J-C plasticity model	A	$324\ MP_a$	$862\ MP_a$
	B	$114\ MP_a$	$331\ MP_a$
	N	0.002	0.34
	C	0.42	0.012
	m	1.34	0.8
Failure model	D_1	-0.77	-0.09
	D_2	1.45	0.27
	D_3	-0.47	0.48
	D_4	0	0.014
	D_5	1.60	3.87
Reference temperature	T_r	$292\ K$	$292\ K$
Bulk speed of sound	v_s	$5240\ m/s$	$5130\ m/s$
Slope of shock velocity versus	S	1.4	1.028
Gruneisen constant	γ_0	1.97	1.23

The Gruneisen EOS is widely used to characterize the relation between the pressure of ductile materials and the rate of change of density under dynamic loading [21]. According to the different metal crystal structures, common metal crystal structures can be classified into three categories: body-centered cubic lattice, face-centered cubic lattice and close-packed hexagonal lattice. The body-centered cubic lattice and the face-centered cubic lattice belong to the cubic crystal system. Since the plasticity of the body-centered cubic lattice is lower than that of the face-centered cubic lattice, the material with face-centered cubic is studied in this work. In order to fully understand the response of different metal crystal structures to a high-speed abrasive particle impacting, the material with close-packed hexagonal is also studied in our work. The material constants of Al6061-T6 and Ti-6Al-4V are listed in Table 1.

2.2 SPH-FEM and boundary conditions

In the AWJ cutting process, the abrasive particles are entrained into the mixing chamber under the Venturi effect and are broken in the cutting head. After passing through the focusing tube, the average size of the abrasive particles is reduced by 35% [5]. In this work, the 80-mesh garnet abrasive is used as the impacting particle. In order to improve the computing efficiency, the deformation and fragmentation of the impacting particle during the erosion process was not considered. The impacting particle is modeled using rigid solid-164 tetrahedral elements, with properties listed in Table 2.

Table 2 Characterization of the abrasive particle for FEA needs [25]

properties	Symbol	Abrasive particle
Particle shape		sphere
particle diameter	d_A	$116\ \mu m$
abrasive density	ρ_A	$4000\ kg/m^3$
elasticity module	E_A	$2.48 \times 10^5\ MP_a$
Poisson's ratio	ν_A	0.27

In this study, the target material is modeled as a rectangular block with the size of $400 * 400 * 200\ \mu m^3$. As mentioned above, the impacting area of the target material is modeled by SPH particles, and the rest is discretized by using the eight-node brick hexahedral elements with one integration point to reduce integration and hourglass control. The impacting area of the target is set to be no less than 1.5 d_A by 1.5 d_A [24]. And it also should not be too large, since the computing efficiency will be too low. Therefore, the SPH particles are distributed in a box with the dimension of $200 * 200 * 100\ \mu m^3$ near the impact location. Considering the calculation time and accuracy, an appropriate spacing of SPH particles needs to be determined. The von Mises stress under different SPH particle spacing ($10\mu m$, $5\mu m$, $4\mu m$ and $3\mu m$) are tested, and the difference between the results of von Mises stress with the spacing of SPH particles under $5\mu m$ and $3\mu m$ is only 0.6%. Thus, the spacing between the SPH particles is determined as $5\mu m$ to compromise between the computation efficiency and relatively high accuracy.

The erosion damage mechanism of ductile materials includes extrusion, cutting, melting, deformation wear, etc. In the AWJ cutting process, various erosion damage mechanisms are caused by various impact angles of abrasive particles. The plastic deformation of material surface caused

by extrusion when the AWJ just touches the target material and the abrasive particles impact the target material at 90-degree impact angle is studied in this paper. Since the eroding process of single abrasive particle at the impact angle of 90° is axisymmetric, $1/4$ geometric model is used to simplify the calculation in this numerical simulation, as illustrated in Fig. 1. Totally, 8,000 SPH particles and 8,166 solid elements are generated by the erosion model.

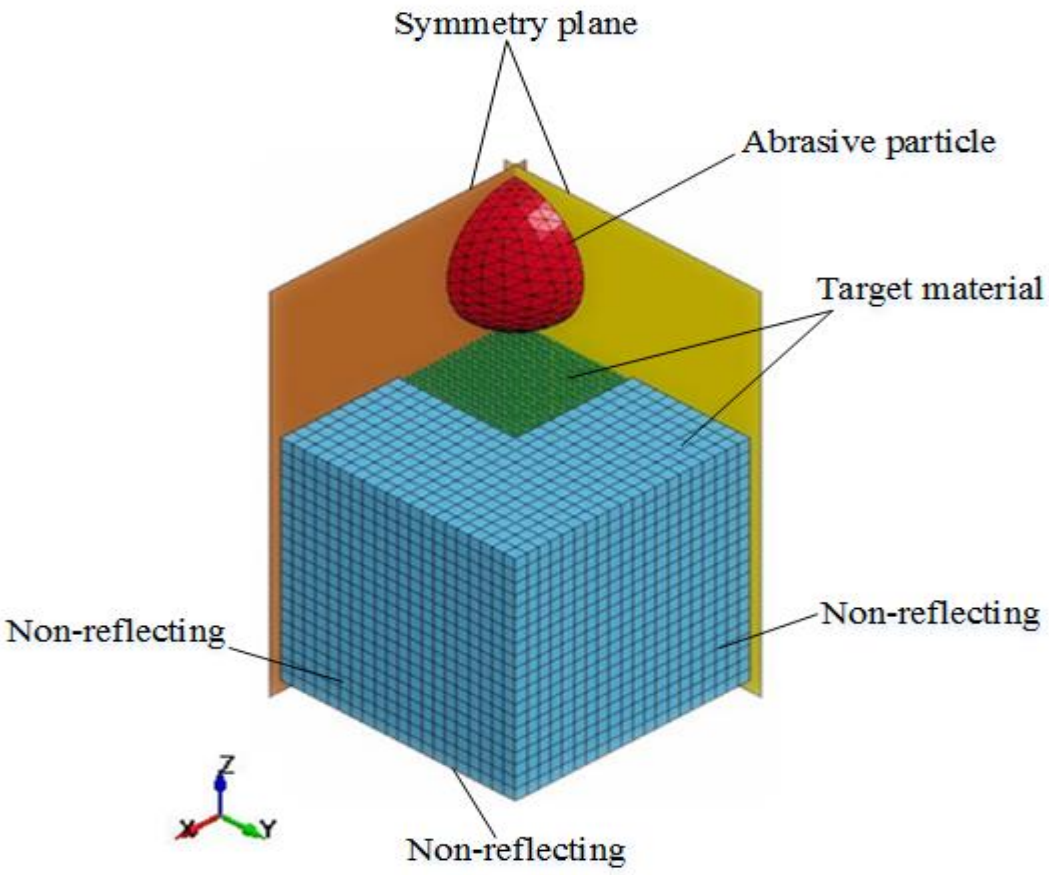

Fig. 1 Model geometry

SPH and FEM are coupled by the master-slave contact algorithm, where the SPH particles are defined as slave segment and the finite elements are set as master segment. The contact coupling algorithm is shown in Fig. 2. In this model, the SPH and FE models are coupled together through the contact type of "TIED_NODES_TO_SURFACE_OFFSET" in LS-DYNA. Similarly, the "EROSING_NODES_TO_SURFACE" is established between the SPH section and the impacting particle. Since only $1/4$ model is analyzed, the XZ and YZ planes are set as symmetry planes and constraints are imposed on the symmetry planes. And the unconstrained boundary conditions are prescribed on the erosion surface of the target material. The "NON_REFLECTING" condition is adopted on the ground and the side of the target material to eliminate the reflection of stress waves, reduce its computational domain, and simulate unlimited boundary [26, 28].

In the AWJ cutting process, the three-phase flow of water, abrasive and air in the cutting head is a fully developed turbulent flow. The laws of conservation of mass, energy and momentum must be followed in the flow process. According to the method proposed by Liu D et al. [29], the impact velocity of single abrasive particle can be estimated as

$$v_{ra} = 0.75v_a \approx 0.75v_o = 33.57\sqrt{P_i} \quad (3)$$

where v_{ra} is the real impact velocity of single particle; v_a is the theoretical impact velocity of single particle; v_o is the velocity of waterjet; and P_i is the fluid pressure at the orifice inlet.

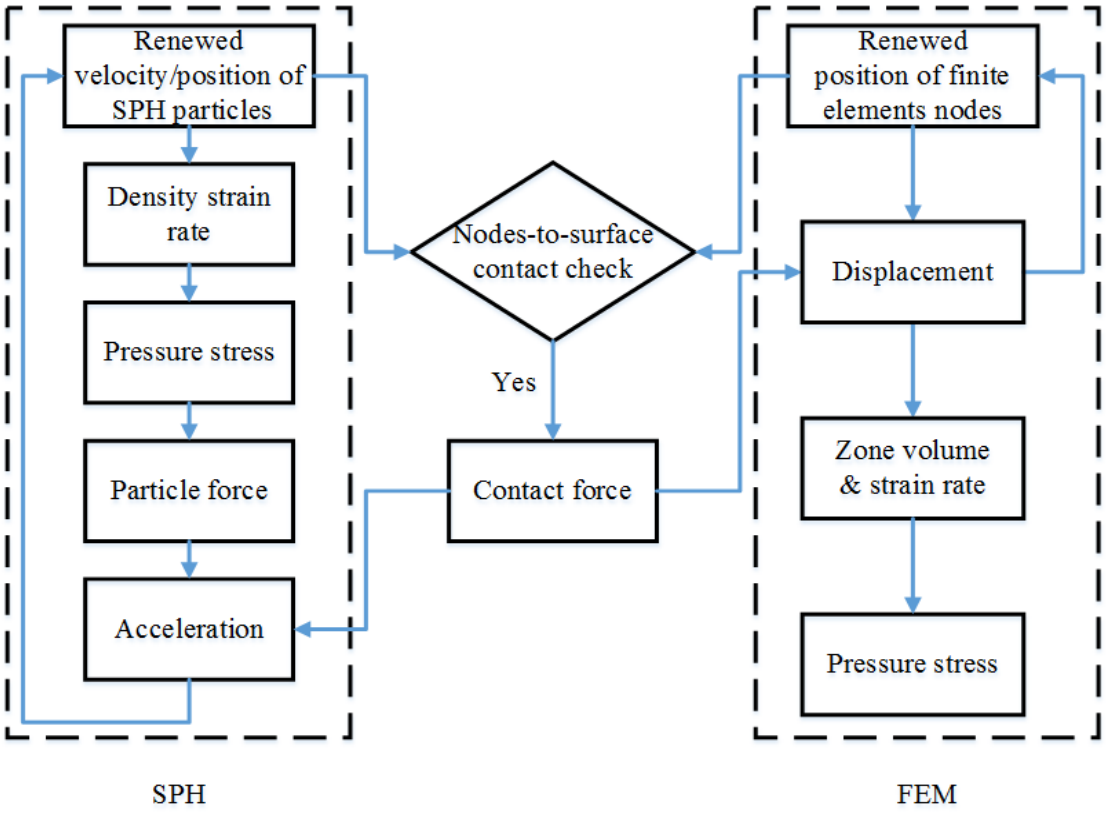

Fig. 2 Coupling SPH with FEA [26-27]

The working pressure range of abrasive water jet cutting process is between 320MP_a and 380MP_a. And the incident velocity of abrasive particle is calculated according to formula (3). Finally, 630m/s is determined as the incident velocity of the impacting particle.

3 Process simulation

In the AWJ cutting process, the erosion damage of ductile materials is affected by many factors including material performance parameters, process parameters, equipment parameters, etc. Among them, the material performance parameters are regarded as the most relevant and essential factor to determine the target damage. Based on the works of Finnie and Bitter et al., whether flow stress, density, specific heat, shear modulus and elastic modulus have effects on erosion damage of the target material from the perspective of material performance parameters is investigated in this work. The effect of the interaction of the material property factors on the erosion damage of the material is further studied.

3.1 Simulation analysis of single factor

In the LS-DYNA software, some simulation experiments were done through the controlled

variable method to study the influence of single material performance factor on the plastic strain of the target. Before the simulation analysis, it can be seen from the flow stress formula (1) that when the constant m increases, the flow stress increases. And the relationship between the flow stress and the target erosion damage can be obtained indirectly. Therefore, the constant m is chosen as an independent variable to explore the effect of flow stress on the erosion damage of target. The variation range of each material property parameter is detailed in Table 3 and Table 4. The simulation results are shown in Fig. 3 and Fig. 4.

It is obvious from Fig. 3 and Fig. 4 that the plastic strain of the target is related to the flow stress, mass density, specific heat and shear modulus, while with nothing to do with Young's modulus. On the whole, the maximum effective plastic strain of the target decreases with the increase of flow stress, mass density and specific heat, and increases with the increase of shear modulus.

Table 3 Each material property parameter and level of Al6061-T6

Level	Constant m	Mass density kg/m^3	specific heat $K/(kg \cdot J)$	shear modulus GP_a	Young's modulus GP_a
1	0.54	2000	635	10	53
2	0.74	2200	695	14	57
3	0.94	2400	755	18	61
4	1.14	2600	815	22	65
5	1.34	2800	875	26	69
6	1.54	3000	935	30	73
7	1.74	3200	995	34	77
8	1.94	3400	1055	38	81
9	2.14	3600	1115	42	85

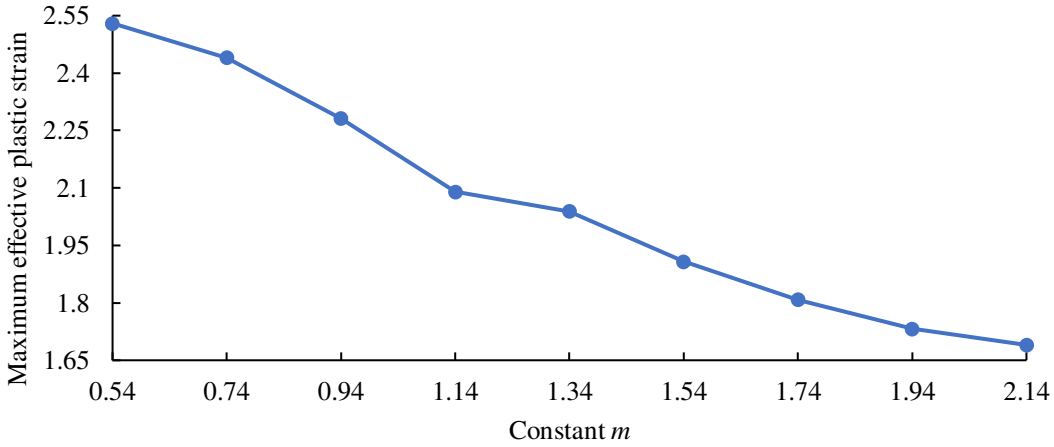

a. Relationship between maximum effective plastic strain and constant *m*

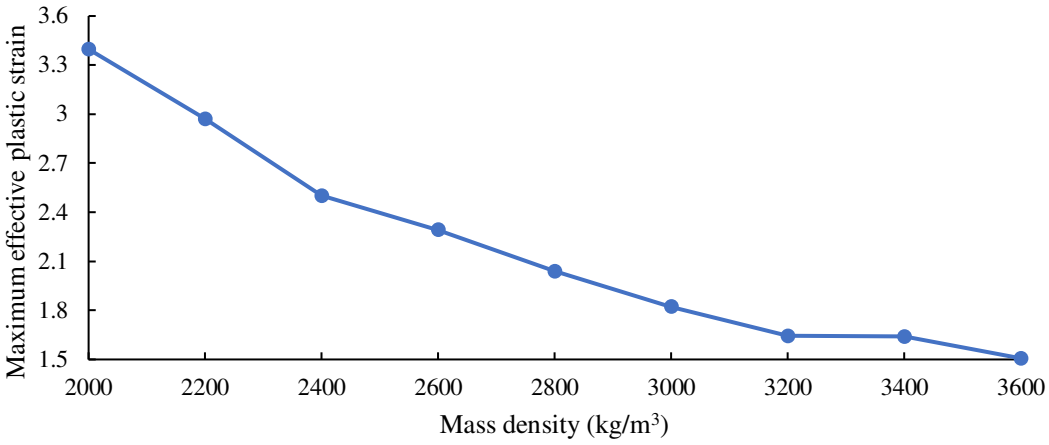

b. Relationship between maximum effective plastic strain and mass density

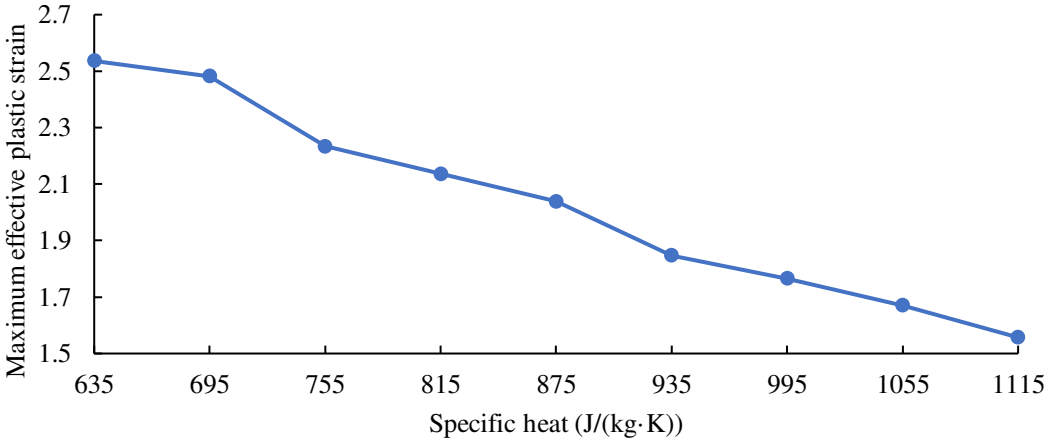

c. Relationship between maximum effective plastic strain and specific heat

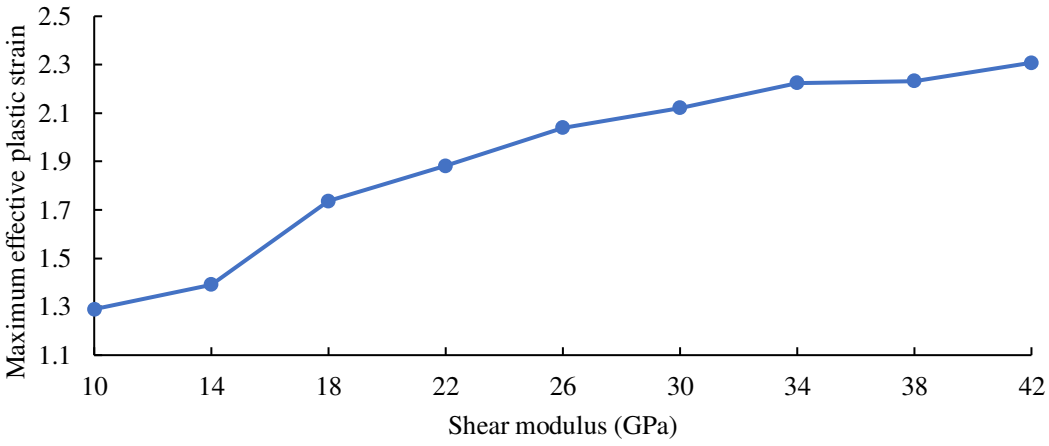

d. Relationship between maximum effective plastic strain and shear modulus

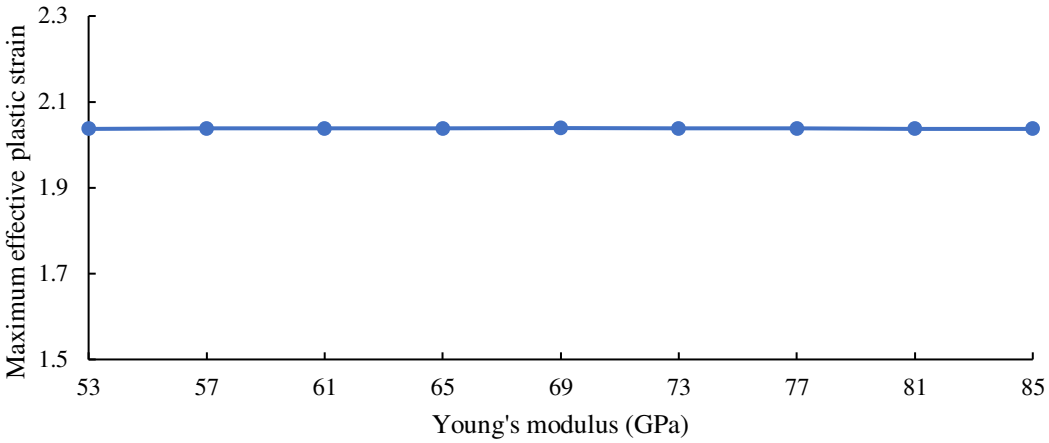

e. Relationship between maximum effective plastic strain and Young's modulus

Fig. 3 Relationship between maximum effective plastic strain and material property parameters of Al6061-T6

Table 4 Each material property parameter and level of Ti-6Al-4V

Level	Constant m	Mass density kg/m^3	Specific heat $K/(kg \cdot J)$	Shear modulus GP_a	Young's modulus GP_a
1	0.2	3628	340	25.9	97.8
2	0.4	3828	400	29.9	101.8
3	0.6	4028	460	33.9	105.8
4	0.8	4228	520	37.9	109.8
5	1.0	4428	580	41.9	113.8
6	1.2	4628	640	45.9	117.8
7	1.4	4828	700	49.9	121.8
8	1.6	5028	760	53.9	125.8
9	1.8	5228	820	57.9	129.8

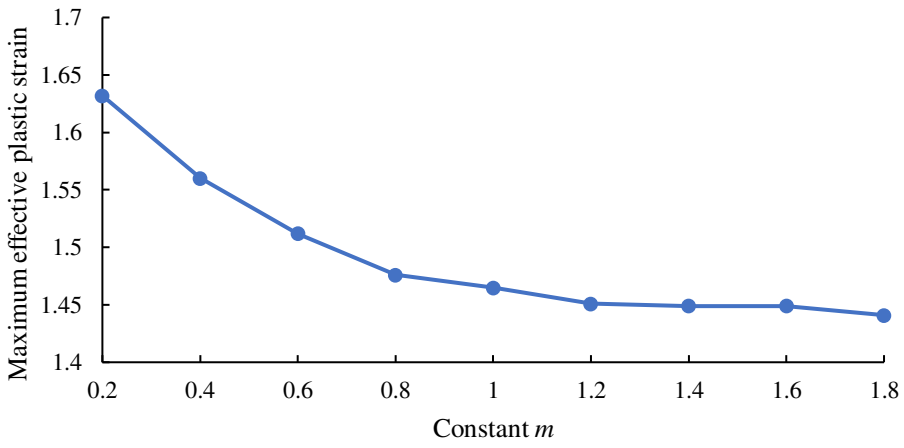

a. Relationship between maximum effective plastic strain and constant m

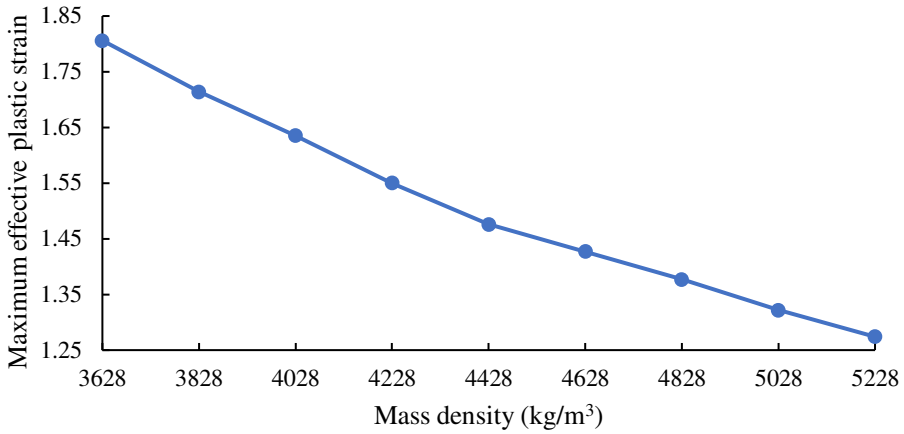

b. Relationship between maximum effective plastic strain and mass density

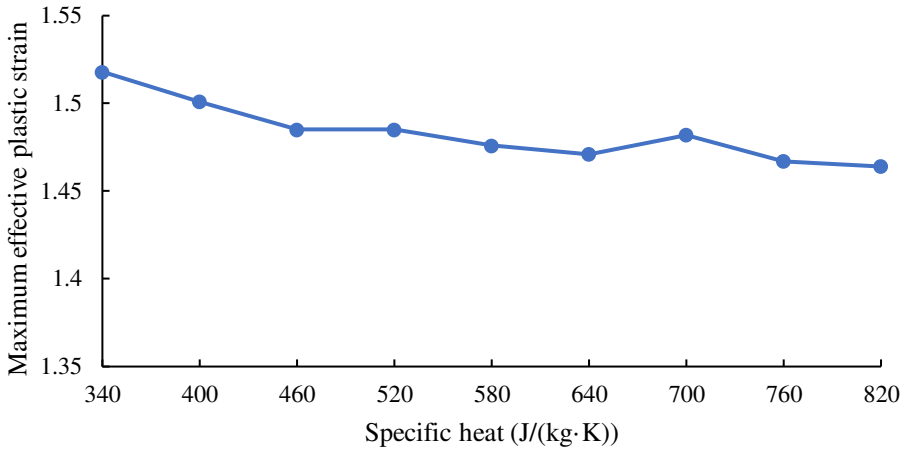

c. Relationship between maximum effective plastic strain and specific heat

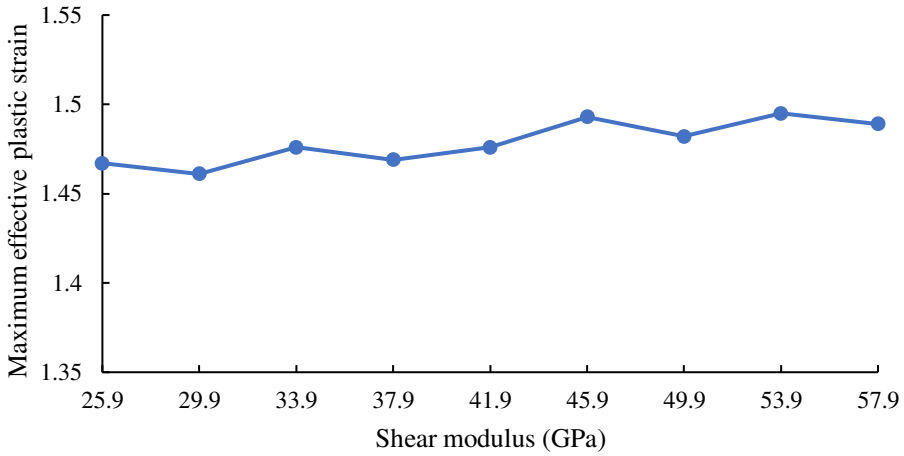

d. Relationship between maximum effective plastic strain and shear modulus

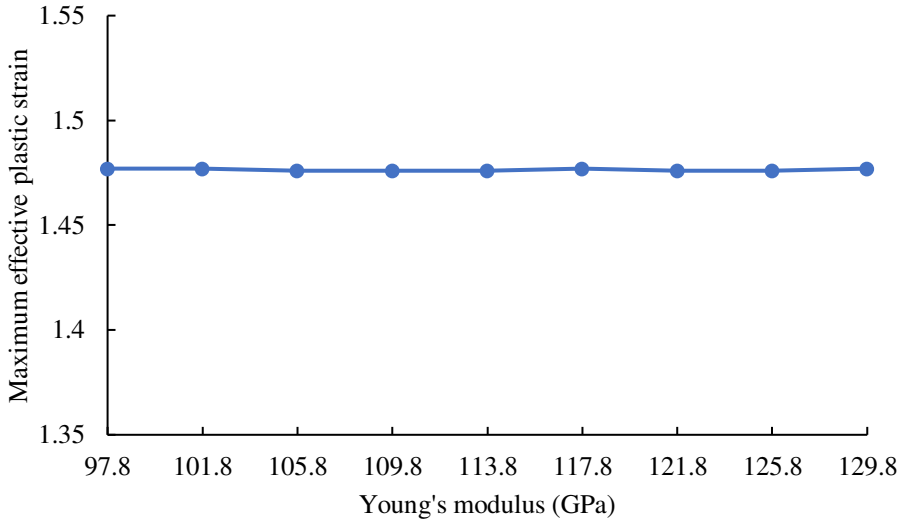

e. Relationship between maximum effective plastic strain and Young's modulus

Fig. 4 Relationship between maximum effective plastic strain and material property parameters of Ti-6Al-4V

3.2 Simulation analysis of multi-factor

In order to reduce the complexity of experiments, the orthogonal experiment method is adopted in this paper to study the influence of the interaction of flow stress, mass density, specific heat and shear modulus on the plastic strain of the target. In order to deeply explore the interrelationship among the material property factors, five experimental levels of each material performance factor are set. And the orthogonal experimental table, $L_{25}(5^6)$, is used as an experimental design scheme. Relevant experimental parameters and levels of Al6061-T6 are listed in Table 5, and the experimental results of orthogonal test are shown in Table 6.

In table 6, A is the constant m, B is the mass density, C is the specific heat, D is the shear modulus, E and F are the blank variables, and S is the maximum effective plastic strain. Analysis of variance is carried out for the orthogonal experimental data. The analysis results are shown in Table 7.

Similarly, the analysis results of variance for Ti-6Al-4V are listed in Table 8.

Table 5 Relevant experiment parameters and levels of Al6061-T6

Level	Constant m	Mass density kg/m^3	Specific heat $K/(kg \cdot J)$	Shear modulus GP_a
1	0.94	2400	755	18
2	1.14	2600	815	22
3	1.34	2800	875	26
4	1.54	3000	935	30
5	1.74	3200	995	34

Table 6 Orthogonal table and the results of simulation experimental of Al6061-T6

Experiment number	*A*	*B*	*C*	*D*	*E*	*F*	*S*
1	1	1	1	1	1	1	2.8317
2	1	2	3	4	5	2	2.61345
3	1	3	5	2	4	3	1.90954
4	1	4	2	5	3	4	2.21868
5	1	5	4	3	2	5	1.90297
6	2	1	5	4	3	5	2.38835
7	2	2	2	2	2	1	2.31087
8	2	3	4	5	1	2	2.15524
9	2	4	1	3	5	3	2.17724
10	2	5	3	1	4	4	1.55748
11	3	1	4	2	5	4	2.25411
12	3	2	1	5	1	5	2.73985
13	3	3	3	3	3	1	2.03584
14	3	4	5	1	2	2	1.33405
15	3	5	2	4	1	3	1.80561
16	4	1	3	5	2	3	2.59611
17	4	2	5	3	1	4	1.94225
18	4	3	2	1	5	5	1.84068
19	4	4	4	4	4	1	1.66755
20	4	5	1	2	3	2	1.79437
21	5	1	2	3	4	2	2.70676
22	5	2	4	1	3	3	1.55298
23	5	3	1	4	2	4	2.21991
24	5	4	3	2	1	5	1.48062
25	5	5	5	5	5	1	1.45444

Table 7 Variance analysis table of Al6061-T6

Independent variable	Sum of square	Freedom	Average square	*F*	Significance
A	0.034	4	0.009	0.788	
B	0.212	4	0.053	26.344	High significance
C	0.003	4	0.001	0.056	
D	0.003	4	0.001	0.051	

Table 8 Variance analysis table of Ti-6Al-4V

Independent variable	Sum of square	Freedom	Average square	*F*	Significance
A	0.496	4	0.124	0.621	
B	2.420	4	0.605	5.848	High significance
C	0.937	4	0.234	1.319	
D	0.564	4	0.141	0.719	

According to the results, mass density has a significant influence on the erosion damage of the target materials, while flow stress, specific heat and shear modulus have a small influence.

4 Conclusion and verification

In this work, a new method called SPH-FEM is used to investigate the influence of the key material property factors of the target materials on the AWJ cutting. The advantage of the SPH-FEM is that it is easy to measure the plastic strain caused by the interaction of these factors under a high-speed abrasive particle impacting on the target materials, which is difficult to determine by the experiment. Utilizing this method, the relationship between the maximum effective plastic strain of the target material and flow stress, mass density, specific heat, shear modulus and Young's modulus is analyzed. And our simulation results highly match the theoretical analysis results obtained by Finnie and Sundararajan, which is helpful to better understand the fundamental mechanisms of erosion in the AWJ cutting process.

In summary, 1) this work proposed a new idea for studying the influence of material factors on the AWJ cutting performance; 2) our simulation results indicated that the plastic strain of the target is related to the flow stress, the mass density, the specific heat, and the shear modulus, but not to the Young's modulus; 3) mass density has a significant influence on the erosion damage of the target materials, whereas the specific heat, and the shear modulus have negligible influence.

Acknowledgements This work was supported by the National Natural Science Foundation of China (Grant No. 52075313).

References

[1] Hashish M (1982) Steel cutting with abrasive waterjet. Proceedings of the 6th International Symposium on Jet Cutting Technology, BHRA, the University of Surry U.K., 1982(April 6-8): 465-487.

[2] Kale A, S.K S, N S, Subbiah R (2020) A review on abrasive water jet machining process and its process parameters. Materials Today: Proceedings 26:1032-1036.

[3] Nyaboro JN, Ahmed MA, El-Hofy H, El-Hofy M (2020) Fluid-structure interaction modeling of the abrasive waterjet drilling of carbon fiber reinforced polymers. Journal of Manufacturing Processes 58:551-562.

[4] Yuvaraj N, Arunkumar N, Nivetha MS, Lina Esther A (2020) Abrasive water jet piercing of inclined holes on ceramic coated nickel superalloy: A preliminary study. Manufacturing Letters 26:59-63.

[5] Anwar S, Axinte DA, Becker AA (2013) Finite element modelling of overlapping abrasive waterjet milled footprints. Wear 303(1-2): 426-436.

[6] Finnie I (1960) Erosion of surfaces by solid particles. Wear 3: 87-103.

[7] Bitter JGA (1963) A study of erosion phenomena. part I, Wear 6: 5-21.

[8] Bitter JGA (1963) A study of erosion phenomena. part II, Wear 6: 169-190.

[9] Hutchings IM (1992) Ductile-brittle transitions and wear maps for the erosion and abrasion of brittle materials. J. Phys. D 25: A212-A221.

[10] Hutchings IM (1981) A model for the erosion of metals by spherical particles at normal incidence. Wear 70(3): 269-281.

[11] Sundararajan G (1983) An analysis of the localization of deformation and weight loss during single-particle normal impact. Wear 84(2): 217-235.
[12] Sundararajan G (1991) The depth of plastic deformation beneath eroded surfaces: The influence of impact angle and velocity, particle shape and material properties. Wear 149(1-2): 129-153.
[13] Li WY, Wang J, Zhu HT, Li HZ, Huang CZ (2013) On ultrahigh velocity micro-particle impact on steels—A single impact study. Wear 305(1-2): 216-227.
[14] Mieszala M, Torrubia PL, Axinte DA, Schwiedrzik JJ, Guo Y, Mischler S, Michler J, Philippe L (2017) Erosion mechanisms during abrasive waterjet machining: model microstructures and single particle experiments. J. Mater. Process. Technol. 247: 92-102.
[15] Barabas SA, Florescu A (2019) Optimization Method of Abrasive Water Jet Cutting of Welded Overlay Materials. Metals 9(10), 1046, doi:10.3390/met9101046.
[16] Zeng J, Determination of machinability and abrasive cutting properties in AWJ cutting, 2007 American WJTA Conference and Expo, August 19-21, 2007, Houston, Texas, Paper 3-B.
[17] Wang W, Wu YJ, Wu H, Yang CZ, Feng QS (2021) Numerical analysis of dynamic compaction using FEM-SPH coupling method. Soil Dynamics and Earthquake Engineering 140:106420.
[18] Lv Z, Hou R, Chen X, Huang C (2019) Numerical research on erosion involved in ultrasonic-assisted abrasive waterjet machining. Int J Adv Manuf Technol 103: 617-630.
[19] Hao GN, Dong XW, Du MC, Li ZL, Dou ZC (2019) A comparative study of ductile and brittle materials due to single angular particle impact. Wear 428-429: 258-271.
[20] Zhao XB, Tang GH, Liu ZG, Zhang YW (2020) Numerical investigation of erosion characteristics of multiple-particle impact on ductile material with patterned surfaces. Powder technology 362: 527-538.
[21] Takaffoli M, Papini M (2012) Numerical simulation of solid particle impacts on Al6061-T6 part I: three-dimensional representation of angular particles. Wear 292-293: 100-110.
[22] Wang YF, Yang ZG (2009) A coupled finite element and meshfree analysis of erosive wear. Tribol Int 42: 373-377.
[23] Dong XW, Liu GR, Li Z, Zeng W (2016) A smoothed particle hydrodynamics (SPH) model for simulating surface erosion by impacts of foreign particles. Tribol Int 95: 267-278.
[24] Woytowitz PJ, Richman RH (1999) Modeling of damage from multiple impacts by spherical particles. Wear 233-235: 120-133.
[25] Junkar M, Jurisevic B, Fajdiga M, Grah M (2006) Finite element analysis of single-particle impact in abrasive water jet machining. International Journal of Impact Engineering 32(7): 1095-1112.
[26] Wang JM, Liu FH, Yu F, Zhang G (2011) Shot peening simulation based on SPH method. Int J Adv Manuf Technol 56: 571-578.
[27] Jiang HG, Zhao HH, Gao KD, Wang OG, Wang YX, Meng DG (2020) Numerical investigation of hard rock breakage by high-pressure water jet assisted indenter impact using the coupled SPH/FEM method. Powder Technology 376: 176-186.
[28] Yu F, Wang JM, Liu FH (2012) Numerical simulation of single particle acceleration process by SPH coupled FEM for abrasive waterjet cutting. Int J Adv Manuf Technol 59: 193-200.
[29] Liu D, Zhu HT, Huang CZ, Wang J, Yao P (2016) Prediction model of depth of penetration for alumina ceramics turned by abrasive waterjet—finite element method and experimental study. Int J Adv Manuf Technol 87: 2673-2682.

Figures

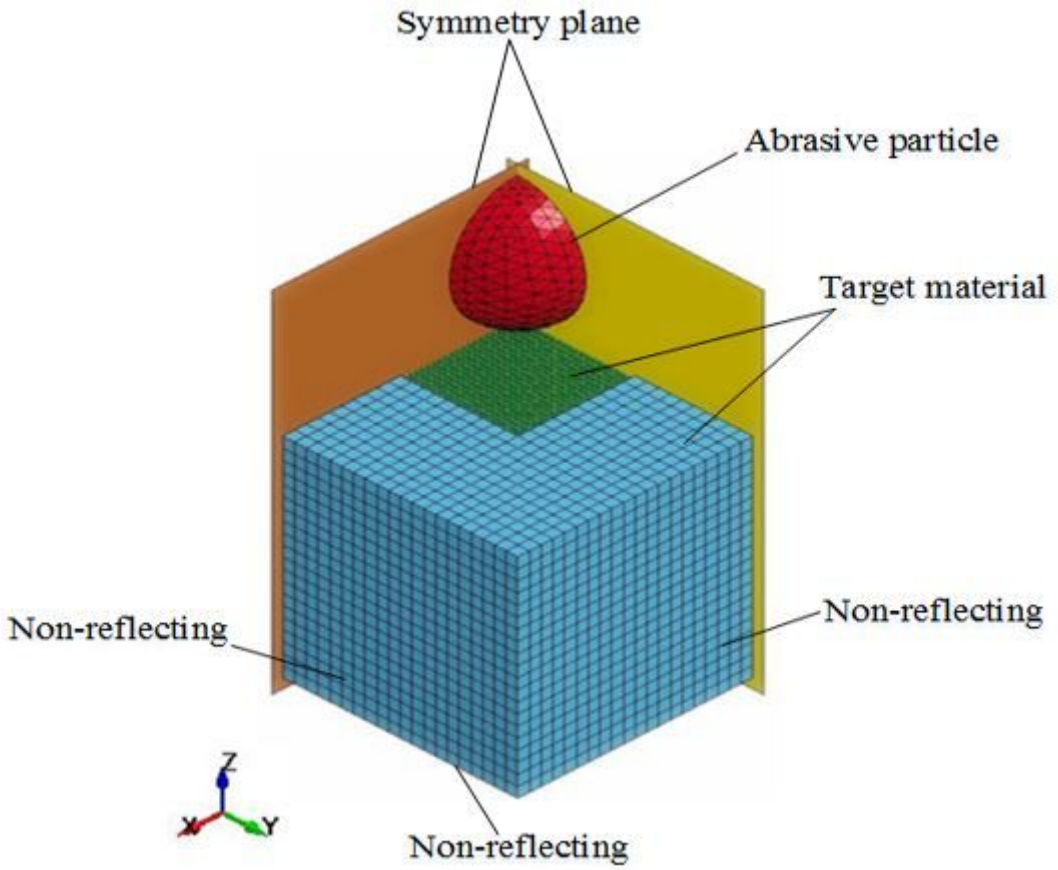

Figure 1

Model geometry

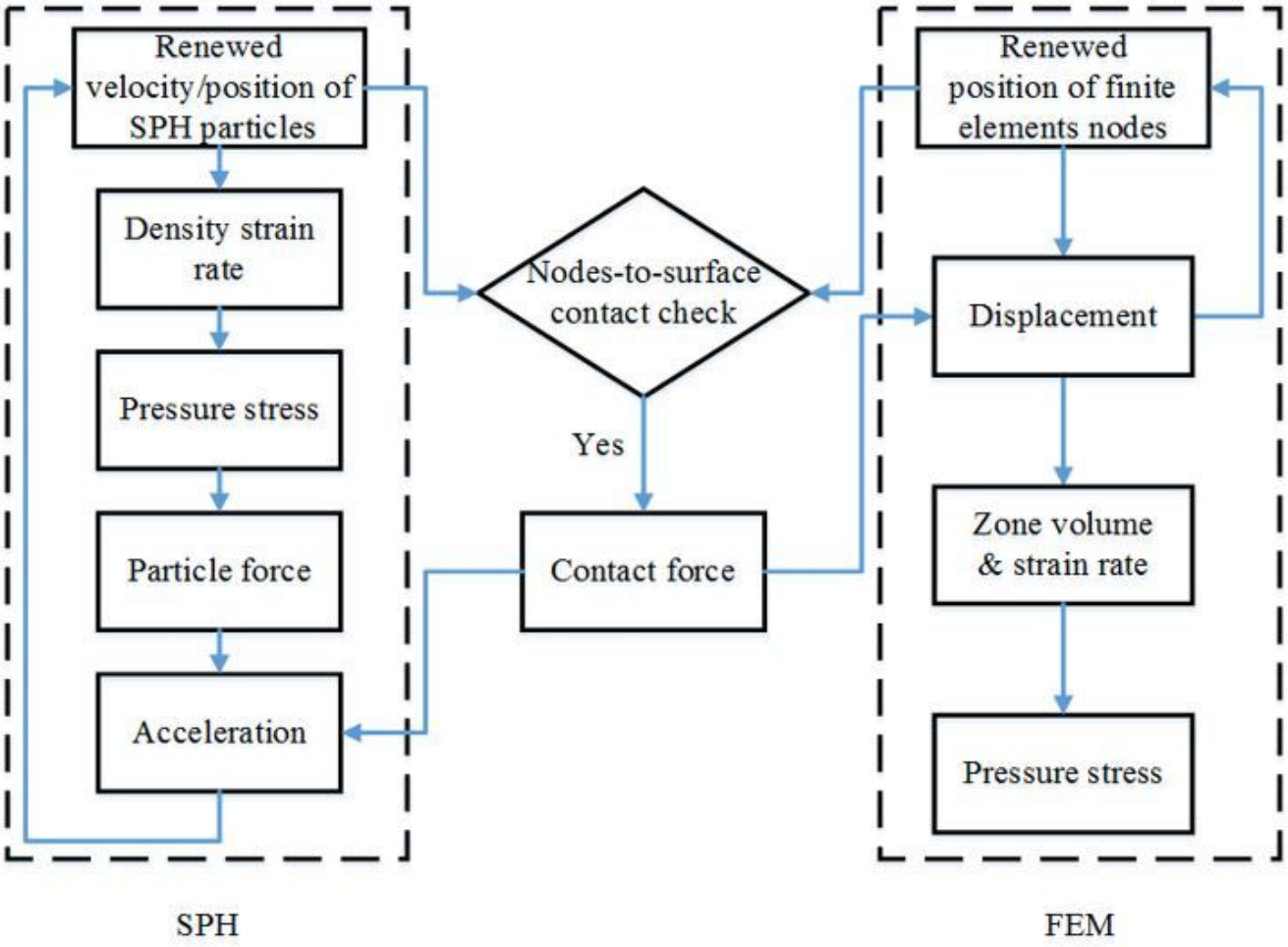

Figure 2

Coupling SPH with FEA [26-27]

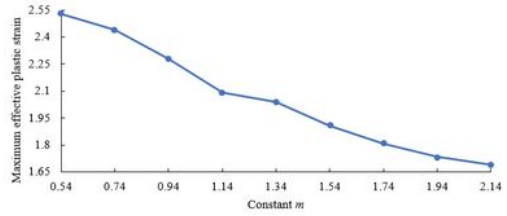

a. Relationship between maximum effective plastic strain and constant m

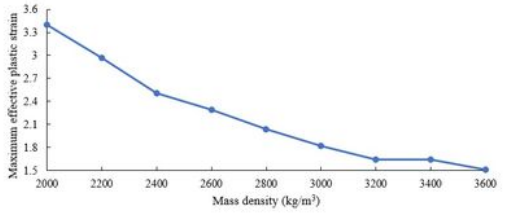

b. Relationship between maximum effective plastic strain and mass density

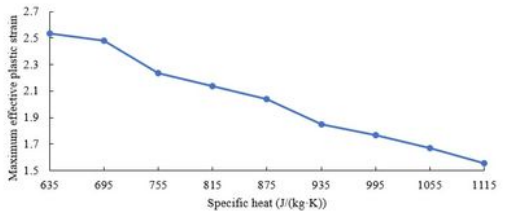

c. Relationship between maximum effective plastic strain and specific heat

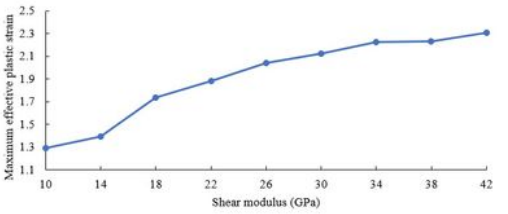

d. Relationship between maximum effective plastic strain and shear modulus

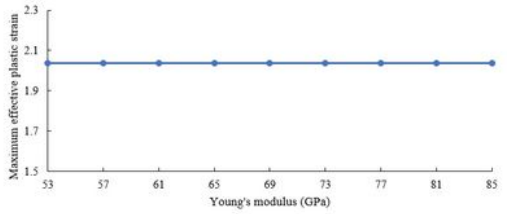

e. Relationship between maximum effective plastic strain and Young's modulus

Figure 3

Relationship between maximum effective plastic strain and material property parameters of Al6061-T6

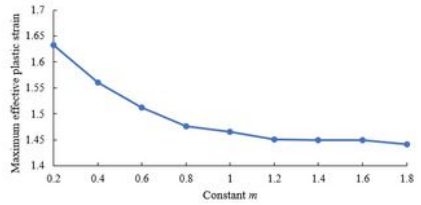

a. Relationship between maximum effective plastic strain and constant m

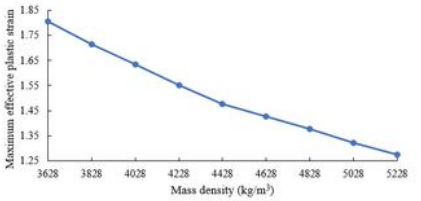

b. Relationship between maximum effective plastic strain and mass density

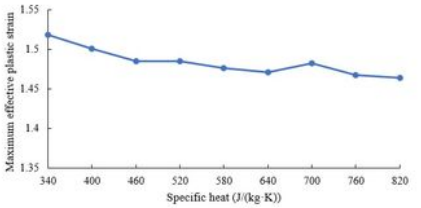

c. Relationship between maximum effective plastic strain and specific heat

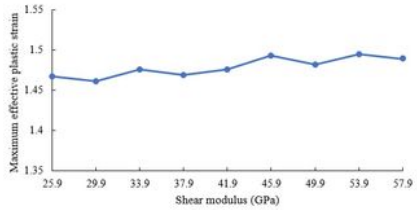

d. Relationship between maximum effective plastic strain and shear modulus

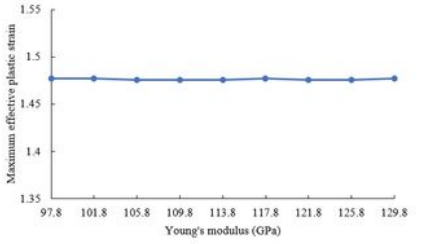

e. Relationship between maximum effective plastic strain and Young's modulus

Figure 4

Relationship between maximum effective plastic strain and material property parameters of Ti-6Al-4V